Original Article

Check for updates

Available online at
www.heca-analitika.com/ijds

Infolitika Journal of Data Science

Vol. 4, No. 1, 2026

Time Series Analysis of UV Radiation and Temperature Using Seasonal ARIMA

Rahmatul Fauzi [1], Tasyaul Husna [1], Izzul Akrami [1], and Novi Reandy Sasmita [1,*]

[1] Department of Statistics, Faculty of Mathematics and Natural Sciences, Universitas Syiah Kuala, Banda Aceh 23111, Indonesia; rahmatulfz@mhs.usk.ac.id (R.F.); husna22@mhs.usk.ac.id (T.H.); izzulakra@mhs.usk.ac.id (I.A.); novireandys@usk.ac.id (N.R.S.)

* Correspondence: novireandys@usk.ac.id

Article History

Received 4 March 2026
Revised 15 May 2026
Accepted 23 May 2026
Available Online 31 May 2026

Keywords:
SARIMA
Time Series
Ultraviolet
Forecasting
Banda Aceh

Abstract

High exposure to ultraviolet (UV) radiation in Banda Aceh poses significant risks to public health and the environment. Daily forecasts of UVA, UVB, and maximum temperature are important for climate planning. But current models often overlook daily changes in tropical regions or fail to incorporate them into their forecasts. This study develops a climatologically informed SARIMA framework incorporating a semiannual seasonal structure (s = 180) to model ultraviolet radiation and temperature dynamics in an equatorial tropical region. The variables used were UVA (W/m^2), UVB (W/m^2), and maximum temperature (°C) in Banda Aceh during the period December 2018-July 2024. The SARIMA method was applied after data pre-processing, such as Box-Cox transformation that stabilizes the variance ($\lambda \approx 1$) and seasonal differencing (s = 180 days) to overcome non-stationarity. Model identification using ACF/PACF plots, with diagnostic tests (Ljung-Box white noise test, Shapiro-Wilk normality test) and accuracy metrics (MAPE, MASE, BIC, and AIC) for optimization. SARIMA$(1,0,2)(1,1,0)^{180}$ was selected as the optimal model for all variables. The selected SARIMA models yielded MAPE values of 18.93% (UVA), 0.48% (UVB), and 13.03% (temperature), indicating that the selected SARIMA specifications were able to capture the dominant temporal patterns observed in the analyzed dataset. The peak values for March-April 2025 were predicted to be 17.69 W/m^2 (UVA), 0.69 W/m^2 (UVB), and 31.85°C.

1. Introduction

As a tropical region located near the equator, Banda Aceh experiences high solar radiation intensity throughout the year, including substantial exposure to ultraviolet (UV) radiation. According to data reported by the Indonesian Meteorological, Climatological, and Geophysical Agency (BMKG), Banda Aceh is among the regions with the highest air temperatures in Indonesia. This condition is primarily attributed to its geographical location within the tropical zone and relatively low cloud cover during certain periods, allowing solar radiation to reach the Earth's surface more intensively. Air temperatures that consistently exceed 34°C indicate significant solar exposure, which is directly associated with elevated levels of ultraviolet radiation.

Ultraviolet radiation consists of Ultraviolet A (UVA), Ultraviolet B (UVB), and Ultraviolet C (UVC), with UVB having the most significant biological impact on human health. Excessive UV exposure can lead to skin damage, premature aging, immune system suppression, and an increased risk of skin cancer [1]. Beyond health implications, extreme UV radiation can also disrupt agricultural productivity and accelerate the degradation of building materials [2]. In the context of climate change

and ozone layer depletion, understanding both daily and seasonal fluctuations of UV radiation has become increasingly important, particularly in densely populated and developing regions such as Banda Aceh.

In Aceh Province, increasing air temperature and prolonged solar exposure have become important environmental concerns. According to BMKG Aceh, several districts in Aceh have experienced repeated extreme temperature events exceeding 34°C during recent dry seasons, particularly under reduced cloud-cover conditions [3]. Prolonged exposure to elevated temperatures and ultraviolet radiation may increase the risk of dehydration, heat stress, and skin-related health problems, particularly among outdoor workers and school-age children in tropical environments [4]. In addition, agricultural activities in Aceh, including rice cultivation and horticultural production, are highly sensitive to temperature variability and excessive solar radiation, which may influence evapotranspiration rates, soil moisture conditions, and crop productivity [5].

Therefore, accurate forecasting of ultraviolet radiation and temperature is relevant not only for scientific climatological analysis but also for practical decision-making. The forecasting outputs generated in this study may support stakeholders such as BMKG Aceh, Dinas Kesehatan Aceh, local disaster mitigation agencies, agricultural planners, and educational institutions in developing adaptive strategies for environmental risk management and climate-related public awareness.

Banda Aceh is located near the equator within the tropical Maritime Continent region, where atmospheric variability is influenced by equinox transitions, monsoonal circulation, and large-scale climate phenomena such as ENSO and the Indian Ocean Dipole (IOD). Unlike subtropical regions that typically exhibit a single annual cycle, equatorial regions frequently experience semiannual variability associated with two annual peaks in solar radiation. These characteristics provide a climatological basis for investigating semiannual seasonal behavior in ultraviolet radiation and temperature time series [6–10].

Mitigating the adverse impacts of UV radiation requires a data-driven and predictive approach. Accurate forecasting of UV radiation and extreme temperatures can support policy planning across multiple sectors, including public health, education, agriculture, and energy. Long-term observational datasets from reliable sources, such as NASA, provide valuable opportunities to develop robust forecasting models. However, the seasonal characteristics and long-term trends inherent in atmospheric data, such as UV radiation and temperature, necessitate appropriate statistical approaches to effectively extract underlying patterns.

Previous studies have applied both statistical and machine-learning approaches for forecasting solar radiation, ultraviolet radiation, and temperature. Machine-learning models such as XGBoost, Random Forest, Long Short-Term Memory (LSTM), and Artificial Neural Networks (ANN) have demonstrated strong predictive performance in environmental forecasting tasks [11–13]. In parallel, statistical time-series models, particularly SARIMA, remain widely used because of their interpretability, computational efficiency, and ability to capture seasonal structures in atmospheric variables [11,14–16].

Several studies have investigated UV radiation forecasting in tropical and subtropical regions. For example, Dabeedoal et al. [11] successfully applied SARIMA and deep learning models to forecast monthly solar radiation and UV index data in Mauritius. However, their study primarily emphasized monthly forecasting performance and did not investigate whether semiannual atmospheric variability linked to equinox-driven solar forcing and monsoonal transitions could constitute a dominant seasonal structure in equatorial tropical environments. Similarly, Chodakowska et al. [12] evaluated ARIMA-based solar radiation forecasting across multiple geographic regions. Other studies have focused primarily on temperature forecasting or broader solar radiation estimation using machine-learning techniques [17,18].

Nevertheless, existing studies predominantly focus on monthly-resolution data, single environmental variables, or non-localized forecasting frameworks. Limited attention has been given to the simultaneous daily forecasting of UVA, UVB, and maximum temperature in tropical coastal regions using long-term high-resolution observations. In particular, studies examining semiannual atmospheric variability in equatorial regions such as Banda Aceh remain scarce. Therefore, this study contributes by integrating multiple atmospheric variables within a daily-resolution SARIMA framework specifically designed for a tropical coastal environment.

The Seasonal Autoregressive Integrated Moving Average (SARIMA) model is a widely used time series approach for data exhibiting both seasonal and trend components [19]. In atmospheric studies, SARIMA has proven effective in capturing periodic patterns and long-term fluctuations, making it a relevant candidate for forecasting variables such as temperature and solar radiation. Furthermore, SARIMA offers advantages in terms of interpretability and computational efficiency compared to black-box

approaches commonly found in machine learning models [15].

Recent forecasting studies have explored approaches such as TBATS, Prophet, LSTM, Transformers, and hybrid SARIMA–machine learning models for handling complex seasonal patterns [20–24]. However, these approaches often require larger datasets and extensive hyperparameter tuning. In contrast, SARIMA remains advantageous for climatological applications because of its interpretability, established statistical diagnostics, and computational efficiency [25,26]. Furthermore, the primary objective of this study is not to benchmark forecasting algorithms, but to characterize and model the semiannual seasonal behavior of ultraviolet radiation and temperature in a tropical coastal region using an interpretable statistical framework. Therefore, SARIMA was considered an appropriate methodological choice for this study despite the relatively long seasonal period (s = 180).

The primary challenge addressed in this study is the development of an accurate and adaptive predictive model for daily UV radiation and temperature in tropical regions. Most existing approaches focus on a single variable or a specific temporal resolution (e.g., monthly data), without integrating UV radiation and temperature by a separate forecasting framework at a daily scale. Such integration is essential to enhance preparedness for extreme weather conditions and associated public health risks.

Although SARIMA has been widely applied in environmental forecasting, studies focusing on daily ultraviolet radiation and maximum temperature in tropical coastal regions remain limited. In particular, the climatic characteristics of Banda Aceh, Indonesia, provide an interesting case for examining semiannual variability in UV radiation and temperature. Therefore, this study applies the SARIMA framework to characterize and forecast these environmental variables using long-term daily observations from NASA POWER.

Specifically, this study utilizes daily data on UVA, UVB, and maximum temperature in Banda Aceh from 2018 to 2024. The dataset, obtained from NASA, has undergone transformation and validation processes to ensure its suitability for analysis. Model selection is conducted through stationarity testing, model identification, and diagnostic evaluation, including white noise and residual normality tests. The optimal model is determined based on performance metrics such as Mean Absolute Percentage Error (MAPE), Mean Absolute Scaled Error (MASE), Bayesian Information Criterion (BIC) and Akaike Information Criterion (AIC).

The objective of this study is to evaluate the applicability of a climatologically informed SARIMA framework for modeling daily ultraviolet radiation and temperature dynamics in Banda Aceh. The primary contribution of this study lies in the development of a climatologically informed SARIMA framework incorporating a semiannual seasonal structure (s = 180) for atmospheric forecasting in equatorial tropical regions. Unlike conventional SARIMA applications that typically assume annual or monthly seasonality, this study demonstrates that semiannual atmospheric variability associated with equinox transitions and monsoonal dynamics may constitute a dominant and physically interpretable seasonal component within the Maritime Continent climate system. Consequently, the study provides methodological insights into the integration of equatorial climatological processes within statistical time-series forecasting frameworks.

2. Materials and Methods

2.1. Data Source

This study employs secondary data consisting of daily observations of Ultraviolet A (UVA), Ultraviolet B (UVB), and maximum temperature in Banda Aceh for the period from December 1, 2018 to July 31, 2024. The dataset was obtained from the NASA Prediction Of Worldwide Energy Resources (POWER) database, which provides reliable satellite-based atmospheric data with daily temporal resolution [27]. These variables were analyzed to develop a forecasting model using the Seasonal Autoregressive Integrated Moving Average (SARIMA) approach.

2.2. SARIMA Model

The SARIMA model extends the Autoregressive Integrated Moving Average (ARIMA) framework to account for seasonal patterns in time series data [28]. The seasonal period in this study was set to s = 180 days to represent the semiannual atmospheric variability commonly observed in equatorial regions such as Banda Aceh. This choice was motivated by equinox-related solar radiation peaks and supported by preliminary inspection of seasonal autocorrelation patterns showing recurring fluctuations approximately every six months [6,8]. Therefore, the selected seasonal period was considered climatologically meaningful for representing tropical atmospheric dynamics. In Banda Aceh, the interaction between equinox-driven solar forcing, monsoonal circulation, and cloud-cover variability may produce two dominant radiation maxima within a year [9]. Consequently, adopting an annual seasonal period (s = 365) have potentially obscure shorter yet physically meaningful atmospheric cycles present in the ultraviolet radiation and temperature series [5,8]. The modeling

Table 1. Theoretical patterns of ACF and PACF for stationary time series.

Model	ACF Pattern	PACF Pattern
AR(p)	Exponential decay (*dies down*)	Sharp cutoff after lag (p)
MA(q)	Sharp cutoff after lag (q)	Exponential decay (*dies down*)
ARMA(p, q)	Exponential decay (*dies down*)	Exponential decay (*dies down*)
AR(p) or MA(q)	Sharp cutoff	Sharp cutoff
White Noise	No significant autocorrelation	No significant autocorrelation

procedure follows the Box–Jenkins methodology, which consists of model identification, parameter estimation, diagnostic checking, and forecasting [29]. The general form of the SARIMA model is given by Equation (1):

$$\Phi_p(B)\Phi_p(B^s)(1-B)^d(1-B^s)^D Xt = \theta_q(B)\theta_q(B^s)\varepsilon_t \qquad (1)$$

where X_t represents the observed time series at time t. $\Phi_p(B)$ and $\Theta_q(B)$ denote the non-seasonal autoregressive (AR) and moving average (MA) components of orders p and q, respectively. $\Phi_P(B^s)$ and $\Theta_Q(B^s)$ represent the seasonal AR and MA components of orders P and Q with seasonal period s. The operators $(1-B)^d$ and $(1-B^s)^D$ correspond to non-seasonal and seasonal differencing, respectively. Finally, ε_t denotes the white noise error term.

2.3. Stationarity Testing

A time series Z_t is considered stationary if its statistical properties, including mean and variance, remain constant over time [30]. When non-stationarity is detected, appropriate transformations are applied to stabilize the series.

2.3.1. Stationarity in Variance

Stationarity in variance is assessed using the Box–Cox transformation. If the estimated parameter $\lambda = 1$, no transformation is required, indicating that the variance is already stable. For $\lambda = 0$, the transformation reduces to the natural logarithm [31]. Otherwise, the data are transformed as shown in Equation (2):

$$\hat{Z}_t = \frac{Z_t^{\lambda} - 1}{\lambda} \qquad (2)$$

2.3.2. Stationarity in Mean

If the series is non-stationary in mean, differencing is applied to achieve stationarity. This process utilizes the backward shift operator B, defined as shown in Equation (3):

$$BZ_t = Z_{t-1} \qquad (3)$$

Thus, the first-order differencing can be expressed as $(1 - B)Z_t$. The differencing process is applied iteratively until the series becomes stationary, which is then statistically verified using the Augmented Dickey–Fuller (ADF) test [12].

2.4. Model Identification

After achieving stationarity, model identification is conducted using the Autocorrelation Function (ACF) and Partial Autocorrelation Function (PACF) plots. The identification of model orders p, q, P, and Q is based on theoretical patterns of ACF and PACF, as summarized in Table 1 [32].

This step enables the selection of candidate SARIMA models based on observed correlation structures. In addition, the seasonal lag structure was inspected through the seasonal ACF pattern. Significant autocorrelation observed around lag 180 provided empirical support for the adoption of a semiannual seasonal period in the SARIMA specification.

2.5. Model Diagnostic Checking

Model adequacy is evaluated through diagnostic testing to ensure that the residuals satisfy statistical assumptions. Parameter significance is assessed using hypothesis testing, where parameters with p-values less than 0.05 are considered statistically significant. Residual independence is evaluated using the Ljung–Box test, which examines whether residuals behave as white noise with zero mean and constant variance [14]. Additionally, the normality of residuals is tested using the Shapiro–Wilk test to verify the assumption of normally distributed errors.

2.6. Model Selection and Evaluation

The optimal SARIMA model is selected by comparing candidate models based on both statistical adequacy and model parsimony. Although parameter significance is considered during model screening, the final model selection is based on information criteria and forecasting accuracy measures. This approach helps avoid overfitting by favoring models that achieve a balance between goodness-of-fit and complexity. In particular, the Akaike Information Criterion (AIC) and Bayesian Information Criterion (BIC) are used to evaluate model parsimony, while forecasting performance is assessed using MASE, and MAPE. The selected SARIMA specification is defined as the one with the lowest AIC, BIC and minimum error values [33]. When disagreements occurred among

Table 2. Descriptive statistics of the variables.

Variables	Minimum	Mean	Median	Standar Deviation	Maximum	Interquartile Range
UVA	2.6	13.6	14.0	2.6	18.5	3.5
UVB	0.1	0.4	0.4	0.1	0.7	0.1
Temperature Max	25.2	29.0	29.0	1.3	33.1	1.8

evaluation metrics, model selection followed a hierarchical decision rule to ensure reproducibility.

First, only models satisfying diagnostic adequacy criteria, including parameter significance, white-noise residuals, and residual normality, were retained. Second, Mean Absolute Scaled Error (MASE) was prioritized as the primary forecasting performance metric because it is scale-independent and generally less sensitive to distortions arising from small magnitudes than percentage-based measures, thereby facilitating more reliable comparisons across time-series variables with different scales. Third, Akaike Information Criterion (AIC) and Bayesian Information Criterion (BIC) were used to evaluate model parsimony, favoring models with lower information criteria when forecasting performance was comparable. Information criteria were considered particularly useful to balance goodness-of-fit and model complexity while reducing overfitting risk. Finally, Mean Absolute Percentage Error (MAPE) was used as a complementary descriptive measure to facilitate interpretation of prediction error and comparability with previous forecasting studies [34–36]. The evaluation metrics for AIC, BIC, MASE, and MAPE are defined as shown in Equation (4)-(7), respectively:

$$AIC = -2ln\,(L) + 2k \tag{4}$$

$$BIC = -2ln(L) + k\,ln\,(n) \tag{5}$$

$$MASE = \frac{MAE}{\frac{1}{n-1}\sum_{t=2}^{n}|Y_t - Y_{t-1}|} \tag{6}$$

$$MAPE = \frac{1}{n}\sum_{t=1}^{n}\left|\frac{Y_t - \hat{Y}_t}{\hat{Y}_t}\right| \tag{7}$$

where Y_t represents the observed value at time t, $\hat{Y}_t$ denotes the predicted value at time t, n is the total number of observations, and $t$indicates the time index. In Equations (4) and (5), L denotes the maximized likelihood function of the fitted model, while k represents the total number of estimated parameters. In Equation (6), MAE refers to the Mean Absolute Error, and the denominator corresponds to the mean absolute difference of consecutive observations in the original time series, which serves as a scaling factor for model comparison.

3. Results and Discussion

3.1. Summary Statistics

Prior to analysis, the dataset underwent several preprocessing and quality-control procedures to ensure its suitability for time series modeling. First, the completeness of the daily observations was evaluated. The NASA POWER dataset used in this study contained no missing values for UVA, UVB, and maximum temperature during the observation period from December 2018 to July 2024. Therefore, no imputation procedure was required.

Data screening was subsequently conducted to identify potential outliers and measurement inconsistencies. Visual inspection using time series plots and boxplots was performed to detect extreme observations. Several unusually high and low values were identified; however, these values were retained because they were climatologically plausible and corresponded to natural atmospheric variability in tropical regions rather than measurement errors.

In addition, descriptive statistical analysis (Table 2) was conducted to summarize the distributional characteristics of each variable, including mean, standard deviation, minimum, and maximum values. This preliminary assessment provided an overview of data variability and supported subsequent stationarity and SARIMA modeling procedures. Since NASA POWER data are satellite-derived and have undergone internal validation and quality assurance procedures by NASA, the dataset is considered reliable for climatological and environmental time series analysis.

3.2. Data Identification

Time series analysis of ultraviolet radiation (UVA and UVB) and maximum temperature was conducted using RStudio. Figure 1 shows that all three variables exhibit clear seasonal patterns. The UVA series (Figure 1a) displays pronounced fluctuations with sharp peaks and troughs, indicating high variability and potential non-stationary behavior. Similarly, the UVB series (Figure 1b) demonstrates recurring cyclical behavior, while the maximum temperature series (Figure 1c) exhibits regular periodic fluctuations that reflect seasonal atmospheric variability. These characteristics justify the application of a seasonal time series approach such as SARIMA.

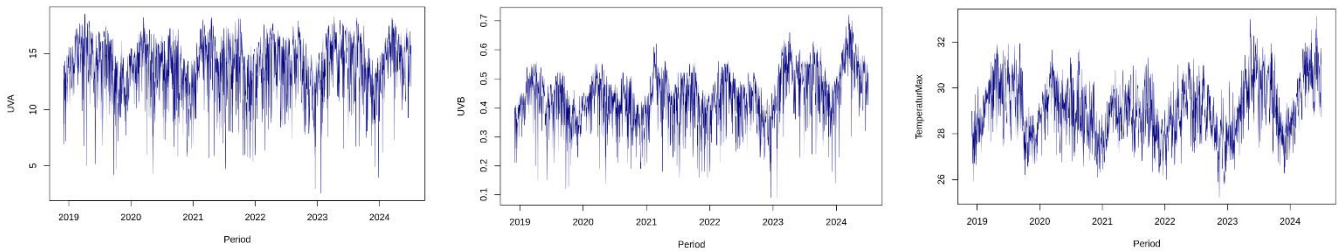

(a) (b) (c)

Figure 1. Time series plots of (a) UVA, (b) UVB, and (c) maximum temperature.

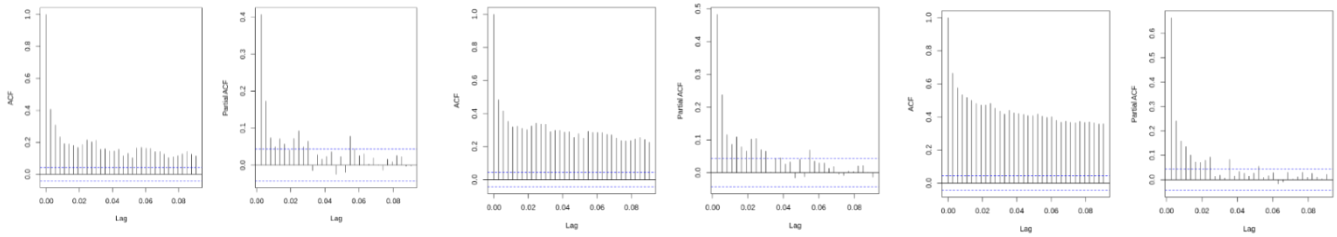

(a) (b) (c)

Figure 2. ACF and PACF plots for (a) UVA, (b) UVB, and (c) maximum temperature.

The observed fluctuations indicate substantial seasonal amplitude in UVA and UVB variability, with recurring peak–trough cycles occurring approximately every six months. Maximum temperature exhibits comparatively smoother oscillations, suggesting greater temporal stability relative to ultraviolet radiation variables. These recurring semiannual patterns provide empirical support for incorporating a seasonal structure into the SARIMA specification.

3.3. Stationarity Testing

3.3.1. Stationarity in Variance

Based on the Box–Cox transformation, the estimated lambda values were 1.092060 (UVA), −0.010737 (UVB), and −0.999924 (maximum temperature). The UVA value, being close to 1, indicates that no transformation was required. In contrast, UVB and temperature required transformation due to non-stationarity in variance. After transformation, the lambda values became 1.000219 (UVB), and 1.000892 (temperature), indicating that variance stationarity was successfully achieved.

3.3.2. Stationarity in Mean

Stationarity in mean was assessed using the Augmented Dickey–Fuller (ADF) test. After applying seasonal differencing ($D = 1$), all variables yielded p-values less than 0.05 (UVA = 0.01, UVB = 0.01, temperature = 0.01). Therefore, the null hypothesis of non-stationarity was rejected, confirming that all series are stationary in mean.

The achievement of stationarity after seasonal differencing further supports the presence of recurrent seasonal behavior in ultraviolet radiation and temperature, indicating that temporal dependence is partly governed by semiannual atmospheric cycles commonly observed in tropical regions [12,20].

3.4. ACF and PACF Analysis

3.4.1. Seasonal Components

Initial model identification was performed using ACF and PACF plots of the stationary series (Figure 2). The ACF and PACF plots at seasonal lags (i.e., multiples of s) indicate the presence of seasonal dependence, suggesting the inclusion of seasonal components in the model. Meanwhile, the behavior of ACF and PACF at lower lags shows gradual decay, indicating that a mixed ARMA structure is appropriate for the non-seasonal components. In particular, the PACF patterns for UVA and UVB exhibit a dominant cutoff around lag 3, indicating the presence of short-term autoregressive dependence. Moreover, significant autocorrelation observed near the seasonal lag supports the inclusion of seasonal SARIMA components and confirms the persistence of semiannual atmospheric cycles in the analyzed variables.

3.4.2. Non-Seasonal Component

To isolate seasonal effects, seasonal differencing with period $s = 180$ was applied. The ACF and PACF plots of the differenced series are shown in Figure 3.

The ACF plots show a gradual decay (tails off), while the PACF plots exhibit a cutoff at lag 3 for UVA and UVB, indicating an autoregressive structure. For maximum temperature, both ACF and PACF display gradual decay,

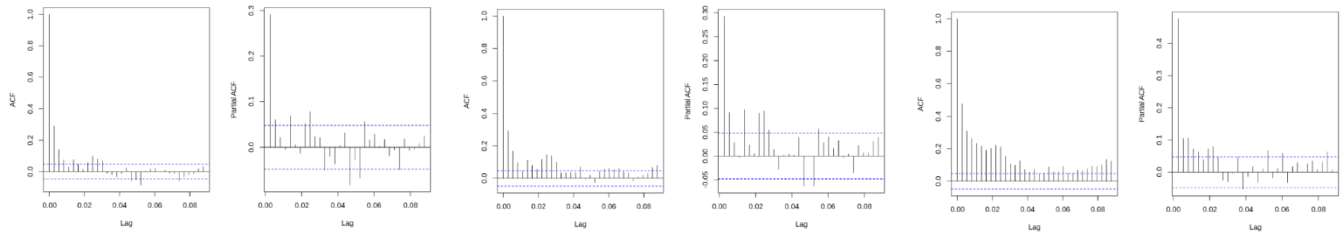

(a) (b) (c)

Figure 3. ACF and PACF plots of seasonally differenced data for (a) UVA, (b) UVB, and (c) maximum temperature.

Table 3. Candidate SARIMA models.

Variable	Model	Specification
UVA	modelUVA1	$SARIMA(1,0,1)(1,1,0)^{180}$
	modelUVA2	$SARIMA(1,0,2)(1,1,0)^{180}$
	modelUVA3	$SARIMA(3,0,1)(0,1,0)^{180}$
	modelUVA4	$SARIMA(1,0,1)(1,0,0)^{180}$
	modelUVA5	$SARIMA(2,0,1)(0,1,0)^{180}$
UVB	modelUVB1	$SARIMA(1,0,1)(1,1,0)^{180}$
	modelUVB2	$SARIMA(1,0,2)(1,1,0)^{180}$
	modelUVB3	$SARIMA(1,0,1)(0,1,1)^{180}$
	modelUVB4	$SARIMA(1,0,1)(1,1,1)^{180}$
	modelUVB5	$SARIMA(2,0,1)(0,1,1)^{180}$
TemperaturMax	modelTemperaturMax1	$SARIMA(1,0,1)(1,1,0)^{180}$
	modelTemperaturMax2	$SARIMA(1,0,2)(1,1,0)^{180}$
	modelTemperaturMax3	$SARIMA(3,0,1)(0,1,0)^{180}$
	modelTemperaturMax4	$SARIMA(1,0,1)(1,0,0)^{180}$
	modelTemperaturMax5	$SARIMA(2,0,1)(0,1,0)^{180}$

suggesting an ARMA structure. These observations guided the selection of candidate SARIMA models.

This pattern indicates that atmospheric variability is not purely random but exhibits temporal persistence, whereby present atmospheric conditions remain partially influenced by preceding states. Similar autocorrelation behavior has been reported in environmental time series characterized by strong seasonal forcing and radiation-driven variability [12,22,25].

3.5. Preliminary Model Identification

Based on the ACF and PACF analysis, several candidate SARIMA models were proposed for each variable (Table 3). These candidate models were selected based on ACF and PACF patterns while maintaining model parsimony. Most candidate models include low-order autoregressive and moving-average terms, reflecting the relatively short-term temporal persistence observed in the atmospheric variables while preserving model simplicity.

3.6. Parameter Significance Testing

Parameter significance was evaluated using p-values, with a threshold of $\alpha = 0.05$. Models with all parameters statistically significant were retained for further analysis.

The results (Table 4) indicate that models UVA1, UVA2, UVA3, UVA5, UVB1, UVB2, UVB3, UVB5, TemperatureMax1, TemperatureMax2, and TemperatureMax5 have all parameters statistically significant ($p < 0.05$) and are therefore considered for diagnostic testing.

3.7. White Noise Test

The Ljung–Box test was applied to evaluate whether residuals behave as white noise (Table 5). A model is considered adequate if the p-value exceeds 0.05.

The results show that all candidate UVA models (UVA1, UVA2, UVA3, and UVA5), UVB2, UVB5, TemperatureMax2, and TemperatureMax5 satisfy the white noise assumption. In contrast, UVB1, UVB3, and TemperatureMax1 fail this criterion and are excluded from further consideration. This step ensures that no significant autocorrelation remains in the residuals.

3.8. Normality Test

Residual normality was assessed using the Shapiro–Wilk test for models that passed the white noise test (Table 6). The results indicate that models UVA1, UVA2, UVA5, UVB2, UVB5, TemperatureMax2, and TemperatureMax5

Table 4. Result of parameter significance test.

Parameter	AR(1)	AR(2)	AR(3)	MA(1)	MA(2)	SAR(1)	SMA(1)
UVA							
UVA1	<0.001	-	-	<0.001	-	<0.001	-
UVA2	<0.001	-	-	<0.001	<0.001	<0.001	-
UVA3	<0.001	<0.001	0.040	<0.001	-	-	-
UVA4	<0.001	-	-	<0.001	-	0.86	-
UVA5	<0.001	<0.001	-	-	<0.001	-	-
UVB							
UVB1	<0.001	-	-	<0.001	-	<0.001	-
UVB2	<0.001	-	-	<0.001	<0.001	<0.001	-
UVB3	<0.001	-	-	<0.001	-	-	<0.001
UVB4	<0.001	-	-	<0.001	-	0.63	<0.001
UVB5	<0.001	<0.001	-	<0.001	-	-	<0.001
Temperatur Max							
TemperaturMax1	<0.001	-	-	<0.001	-	<0.001	-
TemperaturMax2	<0.001	-	-	<0.001	<0.001	<0.001	-
TemperaturMax3	<0.001	<0.001	0.132	<0.001	-	-	-
TemperaturMax4	<0.001	-	-	<0.001	-	0.725	-
TemperaturMax5	<0.001	<0.001	-	<0.001	-	-	-

Table 5. Results of the Ljung–Box test.

Variable	Model	p-value
UVA	modelUVA1	0.6469
	modelUVA2	0.4831
	modelUVA3	0.9907
	modelUVA5	0.6239
UVB	modelUVB1	0.0099
	modelUVB2	0.4616
	modelUVB3	<0.001
	modelUVB5	0.5680
TemperaturMax	modelTemperaturMax1	0.0051
	modelTemperaturMax2	0.6895
	modelTemperaturMax5	0.7703

Table 6. Shapiro–Wilk normality test results.

Variable	Model	SARIMA Model	p-value
UVA	modelUVA1	$(1,0,1)(1,1,0)^{180}$	0.125
	modelUVA2	$(1,0,2)(1,1,0)^{180}$	0.494
	modelUVA3	$(3,0,1)(0,1,0)^{180}$	0.004
	modelUVA5	$(2,0,1)(0,1,0)^{180}$	0.199
UVB	modelUVB2	$(1,0,2)(1,1,0)^{180}$	0.317
	modelUVB5	$(1,0,1)(0,1,1)^{180}$	0.084
TemperaturMax	modelTemperaturMax2	$(1,0,2)(1,1,0)^{180}$	0.131
	modelTemperaturMax5	$(2,0,1)(0,1,0)^{180}$	0.073

Have normally distributed residuals (p-value > 0.05). However, model UVA3 violates the normality assumption and is therefore not considered for the final model selection. Residual normality supports the reliability of statistical inference, although it is not a strict requirement for forecasting performance. Comparatively, the UVA models demonstrated more consistent diagnostic performance across residual independence and normality tests than several UVB and temperature specifications, indicating relatively stronger statistical adequacy for representing ultraviolet radiation dynamics.

3.9. SARIMA Model Selection

When multiple candidate models satisfied all diagnostic criteria, including parameter significance, white noise, and residual normality, the optimal model was determined based on a comparative evaluation of forecasting performance. The selection criteria included

Table 7. Model performance comparison.

Model	MAPE	MASE	AIC	BIC
UVA				
modelUVA1	18.9816	0.7694	10332.8	10354.9
modelUVA2	18.9271	0.7671	10322.2	10349.8
modelUVA5	21.2638	0.8778	10770.3	10792.4
UVB				
modelUVB2	0.4774	0.6244	-12837	-12447.3
modelUVB5	0.5740	0.7508	-12475	-12859.2
TemperaturMax				
TemperaturMax2	13.0329	0.6648	-59991	-59963.6
TemperaturMax5	15.1769	0.7719	-59503	-59481.8

both goodness-of-fit and predictive accuracy measures, namely the Mean Absolute Percentage Error (MAPE), Mean Absolute Scaled Error (MASE), Akaike Information Criterion (AIC), and Bayesian Information Criterion (BIC), as summarized in Table 7. In cases where evaluation metrics yielded conflicting indications, model selection followed the predefined hierarchical decision rule described in Section 2.6, prioritizing MASE, followed by AIC/BIC for model parsimony.

In this study, forecasting evaluation was primarily intended to assess model adequacy and seasonal representation within the observed atmospheric time series through fitted-series evaluation and residual diagnostic consistency, rather than strict out-of-sample predictive benchmarking [12,15,37].

Among the evaluated SARIMA candidate specifications, modelUVA2, modelUVB2, and modelTemperatureMax2 were selected based on the predefined model selection criteria within the SARIMA framework. Specifically, modelUVA2 was selected for UVA, modelUVB2 for UVB, and modelTemperatureMax2 for maximum temperature. The consistency of these results across multiple evaluation metrics suggests that the selected models provide an appropriate balance between model parsimony and goodness-of-fit while adequately representing the temporal dynamics observed in the data. Comparative evaluation further indicates that models with additional seasonal components generally achieved lower forecasting errors and improved information criteria values, supporting the importance of incorporating semiannual atmospheric variability into the SARIMA framework.

Furthermore, model performance was assessed using multiple evaluation metrics, with MASE prioritized for cross-variable comparison due to its scale independence, while MAPE was interpreted cautiously for variables with relatively small magnitudes such as UVB. The selected models yielded relatively low fitted-series forecasting error measures of 18.93% for UVA, 0.48% for UVB, and 13.03% for maximum temperature, although the very low UVB MAPE should be interpreted cautiously due to the relatively small magnitude of UVB observations. Because UVB observations are recorded on a relatively small numerical scale (approximately 0.1–0.7 W/m^2), even very small absolute prediction errors can produce disproportionately low percentage-based error values. Consequently, MAPE may underestimate practical forecasting uncertainty for low-magnitude atmospheric variables and should not be interpreted in isolation [37,38].

Although MAPE is widely used as an indicator of forecasting accuracy, its interpretation should be treated cautiously, particularly for variables with relatively small magnitudes such as UVB. Therefore, model performance was not evaluated solely using MAPE but also through MASE, AIC, and BIC. The consistency of these complementary metrics supports the adequacy of the selected SARIMA specifications for representing the observed temporal patterns. These evaluation measures were interpreted together with residual diagnostic adequacy and climatological consistency to assess the capability of the SARIMA framework in representing dominant temporal dynamics within the available observational dataset [35, 38]. Overall forecasting performance was interpreted primarily using MASE together with diagnostic adequacy criteria rather than relying solely on fixed MAPE thresholds. The relatively low MASE values observed across variables suggest that the selected SARIMA specifications were able to represent the dominant temporal and seasonal dynamics of ultraviolet radiation and temperature while maintaining statistical consistency and climatological interpretability.

3.10. Forecasting Results

Using the selected SARIMA$(1,0,2)(1,1,0)^{180}$ model, forecasts were generated for the next 365 days. The forecasting results reveal consistent seasonal patterns across all variables, aligning with historical observations (Figure 4). Peak values are predicted to occur during March–April 2025, which is climatologically consistent with equinox-related increases in solar radiation and

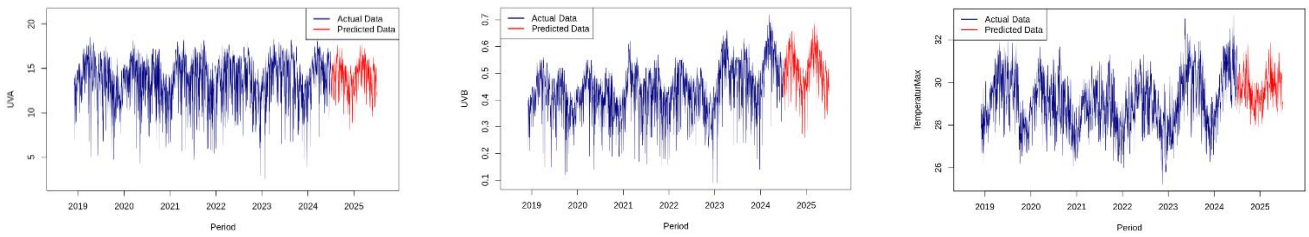

(a) (b) (c)

Figure 4. Forecast results for (a) UVA, (b) UVB, and (c) maximum temperature.

transitional monsoonal conditions in equatorial regions such as Banda Aceh [6,8]. Moreover, the predicted maxima for UVA (17.69 W/m^2), UVB (0.69 W/m^2), and maximum temperature (31.85°C) remain within the historical observation range presented in Table 2, indicating that the forecasts are physically plausible and climatologically realistic.

3.11. Discussion

The results of this study indicate that ultraviolet radiation (UVA and UVB) and maximum air temperature in Banda Aceh exhibit pronounced seasonal behavior that can be represented using SARIMA models with a seasonal period of 180 days. Beyond the statistical performance of the forecasting models, these findings provide important insights into the climatological processes governing environmental variability in equatorial regions.

The identified semiannual seasonality is consistent with the geographical location of Banda Aceh, which lies close to the equator (approximately 5.55°N). In equatorial regions, the apparent position of the sun crosses near the zenith twice each year, around the March and September equinoxes. During these periods, solar irradiance reaching the Earth's surface increases, resulting in elevated levels of ultraviolet radiation and enhanced surface heating. This physical mechanism provides a plausible explanation for the dominant seasonal component captured by the SARIMA models and supports the selection of a seasonal period of 180 days.

From a physical perspective, the autoregressive structure identified in the SARIMA models suggests that atmospheric conditions on a given day are influenced by preceding environmental states, reflecting temporal persistence in radiation and temperature processes. Meanwhile, the seasonal components indicate the recurrence of climatological forcing associated with semiannual solar variability and monsoonal transitions, which repeatedly shape ultraviolet radiation and temperature dynamics in equatorial regions [12,20].

In addition to solar geometry, atmospheric conditions associated with the Asian–Australian monsoon system contribute to variations in surface radiation. Seasonal changes in cloud cover, humidity, and precipitation influence the amount of solar radiation that reaches the surface. During periods characterized by increased cloudiness and rainfall, incoming ultraviolet radiation is attenuated through scattering and absorption processes within the atmosphere. Conversely, clearer atmospheric conditions permit greater transmission of solar radiation, leading to higher UV intensity and warmer surface temperatures. These interactions help explain the observed synchronization between UV radiation and temperature fluctuations throughout the study period.

The forecasting results suggest that semiannual atmospheric variability constitutes a dominant climatological feature captured effectively by the SARIMA framework. This finding demonstrates the importance of considering local climatological characteristics when developing forecasting models for environmental variables.

From a methodological perspective, the present findings suggest that conventional annual seasonal assumptions commonly adopted in atmospheric SARIMA studies may not always be appropriate for equatorial regions characterized by bimodal climatological variability. The identified semiannual structure (s = 180) reflects a physically interpretable representation of equinox-driven atmospheric forcing and therefore may provide a useful alternative framework for environmental forecasting studies conducted within the Maritime Continent and other equatorial tropical regions.

The results also have practical implications. Accurate forecasting of ultraviolet radiation can support public health initiatives related to UV exposure risk, while temperature forecasts can contribute to environmental monitoring, agriculture, and urban planning activities. Given the growing concern regarding climate variability and its impacts on human activities, reliable forecasting tools based on historical atmospheric observations may assist decision-makers in developing adaptive strategies.

In practical implementation, the forecasting outputs generated in this study may support operational

environmental monitoring conducted by BMKG Aceh, particularly during periods characterized by elevated ultraviolet radiation and high surface temperature. Forecast information indicating sustained increases in UVA and UVB levels during equinox-transition months may be used to strengthen public heat-exposure advisories, outdoor activity recommendations, and climate-risk communication strategies. In the agricultural sector, forecasts of prolonged high-temperature conditions may assist local agricultural agencies in anticipating irrigation demand, evapotranspiration stress, and crop exposure risks during dry periods.

Although no universal operational threshold currently exists for localized ultraviolet forecasting in Banda Aceh, periods exhibiting simultaneously elevated UV radiation and maximum temperature may represent environmentally sensitive conditions requiring increased public awareness. Therefore, the forecasting framework developed in this study may contribute to climate adaptation planning and environmental early-warning support systems in tropical coastal regions.

Future work may complement quantitative evaluation by incorporating visual validation tools, including actual-versus-predicted plots, prediction intervals, and extended residual diagnostics to further assess forecasting uncertainty and model adequacy [36,37].

The identified semiannual seasonal behavior is broadly consistent with previous studies conducted in tropical and subtropical regions. For example, studies on solar radiation forecasting in tropical environments have similarly reported strong seasonal dependencies associated with solar geometry and atmospheric variability [11,12]. Likewise, recent forecasting studies comparing SARIMA and alternative approaches in tropical climates have shown that seasonal autoregressive structures are effective for representing recurring atmospheric cycles in temperature and radiation-related variables [40,41]. The consistency between the present findings and prior tropical studies strengthens the climatological plausibility of the identified seasonal dynamics in Banda Aceh.

The emergence of the same SARIMA structure across UVA, UVB, and maximum temperature may reflect their shared dependence on common atmospheric forcing mechanisms, particularly semiannual solar geometry and monsoonal variability in equatorial regions. Although these variables differ physically, they are influenced by closely related climatological cycles, which may explain the similar autoregressive and seasonal dependence structures identified in this study [12,22,25].

Despite the favorable diagnostic and forecasting results obtained in this study, several methodological and climatological limitations should be acknowledged. Since SARIMA relies primarily on historical temporal patterns, the model may have limited capability in representing abrupt atmospheric anomalies or extreme climate events that deviate substantially from historical behavior. In addition, long-term climate variability and climate change may influence the stationarity assumption underlying the SARIMA framework, potentially affecting forecasting stability over extended periods. Forecast uncertainty also generally increases as the prediction horizon becomes longer, particularly for forecasts approaching the 365-day horizon. Nevertheless, the forecasting results may still provide practical value for environmental monitoring, UV exposure awareness, and temperature-related risk communication by regional agencies such as BMKG and local public health authorities in Aceh. Future research may therefore explore hybrid forecasting approaches incorporating exogenous atmospheric variables such as cloud cover, humidity, precipitation, aerosol concentration, ENSO indices, and Indian Ocean Dipole (IOD) indicators to improve forecasting robustness under evolving climatic conditions. Future studies may also investigate whether the semiannual seasonal structure identified in Banda Aceh is reproducible across other equatorial tropical cities within the Maritime Continent region. Comparative multi-location analyses could provide broader evidence regarding the climatological generalizability of semiannual atmospheric forecasting frameworks in tropical environments. Future studies may further evaluate forecasting robustness using rolling-origin validation or alternative time-series cross-validation strategies under varying atmospheric conditions [38].

4. Conclusions

This study demonstrates that the SARIMA$(1,0,2)(1,1,0)^{180}$ model provides a robust and statistically valid framework for forecasting daily UVA, UVB, and maximum temperature in Banda Aceh using NASA POWER data from December 1, 2018 to June 30, 2024. The model satisfies all diagnostic assumptions, including parameter significance, white noise residuals, and normality, indicating its adequacy for time series forecasting.

Forecasting results for the period July 1, 2024 to June 30, 2025 (365 days ahead) indicate that peak values are expected to occur during March–April 2025, with predicted maxima of 17.69 W/m² for UVA, 0.69 W/m² for UVB, and 31.85°C for maximum temperature. These results confirm the presence of strong semiannual seasonal patterns in ultraviolet radiation and temperature dynamics in tropical regions, which are

climatologically consistent with equinox transitions and monsoonal variability in Banda Aceh. Furthermore, the predicted peak values remain within the historical observation range, supporting the physical plausibility of the forecasts.

Model performance evaluation shows Mean Absolute Percentage Error (MAPE) values of 18.93% for UVA, 0.48% for UVB, and 13.03% for maximum temperature. Forecasting performance evaluation based primarily on MASE and supported by diagnostic adequacy tests indicates that the selected SARIMA models were able to represent the dominant temporal dynamics of UVA, UVB, and maximum temperature in Banda Aceh. Although MAPE values were also reported for comparability with previous forecasting studies, their interpretation was treated cautiously for low-magnitude variables such as UVB.

Overall, the findings confirm that the SARIMA approach is effective in capturing both seasonal and short-term dynamics of atmospheric variables in a tropical context. This study contributes to the literature by integrating UV radiation and temperature forecasting at a daily resolution, offering practical implications for climate adaptation strategies, public health risk mitigation, and environmental management in regions with high solar exposure.

Beyond the local forecasting application, this study contributes to the broader environmental forecasting literature by demonstrating that semiannual seasonal structures may constitute a physically meaningful alternative to conventional annual seasonality in equatorial atmospheric time series. Unlike previous tropical SARIMA studies, including Dabeedoal et al. [11], which primarily focused on monthly-resolution forecasting and conventional seasonal specifications, the present study emphasizes climatologically informed seasonal modeling at daily temporal resolution. The identification of a dominant semiannual seasonal structure (s = 180) suggests that atmospheric variability in equatorial Maritime Continent regions may be governed more strongly by equinox-related transitions and monsoonal dynamics than by a single annual cycle.

Nevertheless, several limitations should be considered when interpreting the present findings. Because the SARIMA framework relies primarily on historical temporal dependence, the model may have limited capability in representing abrupt atmospheric anomalies or nonlinear climate dynamics. Furthermore, the absence of exogenous atmospheric predictors such as cloud cover, humidity, and large-scale climate indices may restrict the model's ability to capture complex environmental forcing mechanisms.

Although the specific SARIMA$(1,0,2)(1,1,0)^{180}$ configuration identified in this study should not be interpreted as universally transferable to all tropical regions, the methodological framework developed here may be generalized to other equatorial environments exhibiting bimodal atmospheric variability. Therefore, the primary scientific contribution of this study lies not merely in the forecasting results themselves, but in the climatologically grounded integration of semiannual atmospheric dynamics into the SARIMA modeling framework for tropical ultraviolet radiation and temperature forecasting. Future research is therefore recommended to investigate hybrid SARIMA–machine learning approaches, incorporate exogenous climate variables, and evaluate the applicability of semiannual forecasting structures across multiple equatorial tropical regions within the Maritime Continent.

Author Contributions: Conceptualization, R.F., T.H. and N.R.S; methodology, N.R.S, and T.H.; software, I.A.; validation, R.F., and T.H.; formal analysis, N.R.S, and R.F.; investigation, T.H.; resources, I.A.; data curation, N.R.S., and I.A.; writing—original draft preparation, N.R.S., and R.F.; writing—review and editing, N.R.S., R.F., and T.H.; visualization, I.A.; supervision, N.R.S.; project administration, R.F. All authors have read and agreed to the published version of the manuscript.

Funding: This study does not receive external funding.

Ethical Clearance: Not applicable

Informed Consent Statement: Not applicable

Data Availability Statement: Data is available upon request to the authors.

Acknowledgments: The authors would like to express their sincere gratitude to all parties who contributed to the completion of this study. Special appreciation is extended to the academic supervisors for their valuable guidance, constructive feedback, and continuous support throughout the research process. The authors also acknowledge NASA POWER for providing accessible and reliable atmospheric data used in this study.

Conflicts of Interest: All the authors declare no conflicts of interest.

References

1. Snyder, A., Valdebran, M., Terrero, D., Amber, K. T., and Kelly, K. M. (2020). Solar Ultraviolet Exposure in Individuals Who Perform Outdoor Sport Activities, *Sports Medicine - Open*, Vol. 6, No. 1, 42. doi:10.1186/s40798-020-00272-9.

2. Arijaje, T. E., Omotosho, T. V., Akinwumi, S. A., Ometan, O. O., and Fashade, O. O. (2022). Analysis of Solar Ultraviolet Radiation Index over Nigeria, West Africa, *IOP Conference Series: Earth and Environmental Science* (Vol. 993), IOP Publishing, Ota, Nigeria, 1–12. doi:10.1088/1755-1315/993/1/012025.

3. Voice of Indonesia. (2025). BMKG Detects 32 Hotspots Across Aceh as Dry Season Intensifies.
4. Kunda, J. J., Gosling, S. N., and Foody, G. M. (2024). The Effects of Extreme Heat on Human Health in Tropical Africa, *International Journal of Biometeorology*, Vol. 68, No. 6, 1015–1033. doi:10.1007/s00484-024-02650-4.
5. Ferijal, T., and Fauzi, A. (2024). Analysis of Local Climate Change Impacts on the Rainfall Patterns and Dry Spells in Banda Aceh and Aceh Besar, Indonesia, *International Journal of Design & Nature and Ecodynamics*, Vol. 19, No. 3, 947–954. doi:10.18280/ijdne.190324.
6. Zul, A., Zaini, A., Vonnisa, M., Marzuki, M., and Ramadhan, R. (2023). Seasonal Variation of Rainfall in Indonesia under Normal Conditions without ENSO and IOD Events from 1981-2021, *Journal of Research in Science Education*, Vol. 9, No. 11, 9899–9909. doi:10.29303/jppipa.v9i11.4569.
7. Supari, Tangang, F., Juneng, L., and Aldrian, E. (2017). Observed Changes in Extreme Temperature and Precipitation over Indonesia, *International Journal of Climatology*, Vol. 37, No. 4, 1979–1997. doi:10.1002/joc.4829.
8. Cai, W., Santoso, A., Collins, M., Dewitte, B., Karamperidou, C., Kug, J.-S., Lengaigne, M., McPhaden, M. J., Stuecker, M. F., Taschetto, A. S., Timmermann, A., Wu, L., Yeh, S.-W., Wang, G., Ng, B., Jia, F., Yang, Y., Ying, J., Zheng, X.-T., et al. (2021). Changing El Niño–Southern Oscillation in a Warming Climate, *Nature Reviews Earth & Environment*, Vol. 2, No. 9, 628–644. doi:10.1038/s43017-021-00199-z.
9. Ratna, S. B., Cherchi, A., Osborn, T. J., Joshi, M., and Uppara, U. (2021). The Extreme Positive Indian Ocean Dipole of 2019 and Associated Indian Summer Monsoon Rainfall Response, *Geophysical Research Letters*, Vol. 48, No. 2, 1–11. doi:10.1029/2020GL091497.
10. Deshafa, A. F. (2025). ENSO and IOD Variability: Impacts on Precipitation and Sea Surface Temperature in Bali and NTB, *Journal of the Physical Society of Indonesia*, Vol. 1, No. 1, 13–25. doi:10.35895/jpsi.1.1.13-25.2025.
11. Dabeedoal, J., Boojhawon, R., Gukhool, O., and Shrestha, D. (2023). A Comparative Study of Deep Learning Algorithms and SARIMA Models for Forecasting Monthly Solar Radiation and UV Index: Case Study for Mauritius, *Proceedings of the 7th International Conference on Intelligent Computing and Optimization 2023 (ICO2023), Volume 1*, Springer, Hua Hin, Thailand, 273–283. doi:10.1007/978-3-031-36246-0_26.
12. Chodakowska, E., Nazarko, J., Nazarko, Ł., Rabayah, H. S., Abendeh, R. M., and Alawneh, R. (2023). ARIMA Models in Solar Radiation Forecasting in Different Geographic Locations, *Energies*, Vol. 16, No. 13, 1–24. doi:10.3390/en16135029.
13. Segurado, R., Pereira, S., Correia, D., and Costa, M. (2019). Techno-Economic Analysis of a Trigeneration System Based on Biomass Gasification, *Renewable and Sustainable Energy Reviews*, Vol. 103, No. 1, 501–514. doi:10.1016/j.rser.2019.01.008.
14. Imro'ah, N., Huda, N. M., Utami, D. S., Umairah, T., and Arini, N. F. (2024). Control Chart for Correcting the ARIMA Time Series Model of GDP Growth Cases, *JTAM (Jurnal Teori Dan Aplikasi Matematika)*, Vol. 8, No. 1, 312. doi:10.31764/jtam.v8i1.19612.
15. Shad, M., Sharma, Y. D., and Singh, A. (2022). Forecasting of Monthly Relative Humidity in Delhi, India, Using SARIMA and ANN Models, *Modeling Earth Systems and Environment*, Vol. 8, No. 4, 4843–4851. doi:10.1007/s40808-022-01385-8.
16. Zamri, N. R., and Azmi, N. N. K. (2021). Global Warming in Cameron Highlands: Forecasting Its Temperature Level via ARIMA vs ARAR, *Journal of Physics: Conference Series*, Vol. 1, No. 1, 1–12. doi:10.1088/1742-6596/2084/1/012009.
17. Huang, L., Kang, J., Wan, M., Fang, L., Zhang, C., and Zeng, Z. (2021). Solar Radiation Prediction Using Different Machine Learning Algorithms and Implications for Extreme Climate Events, *Frontiers in Earth Science*, Vol. 9, No. 1, 1–17. doi:10.3389/feart.2021.596860.
18. Benti, N. E., Chaka, M. D., and Semie, A. G. (2023). Forecasting Renewable Energy Generation with Machine Learning and Deep Learning: Current Advances and Future Prospects, *Sustainability*, Vol. 15, No. 9, 7087. doi:10.3390/su15097087.
19. Şenyapar, H. N. D., and Aksoz, A. (2024). Empowering Sustainability: A Consumer-Centric Analysis Based on Advanced Electricity Consumption Predictions, *Sustainability*, Vol. 16, No. 7, 1–23. doi:10.3390/su16072958.
20. Chudo, S. B., and Terdik, G. (2025). Modeling and Forecasting Time-Series Data with Multiple Seasonal Periods Using Periodograms, *Econometrics*, Vol. 13, No. 2, 14–27. doi:10.3390/econometrics13020014.
21. Ahmad, J., Ahmad, I., Miao, Q., and Su, Z. (2025). Forecasting the Human Cost of Disasters under Sustainable Development Goal: A Time Series Analysis Using Facebook Prophet Model, *Technology in Society*, Vol. 83, No. 1, 102–115. doi:10.1016/j.techsoc.2025.102992.
22. Tian, J., Ooka, R., and Lee, D. (2023). Multi-Scale Solar Radiation and Photovoltaic Power Forecasting with Machine Learning Algorithms in Urban Environment: A State-of-the-Art Review, *Journal of Cleaner Production*, Vol. 426, No. 1, 139–150. doi:10.1016/j.jclepro.2023.139040.
23. Yemets, K., Izonin, I., and Dronyuk, I. (2025). Time Series Forecasting Model Based on the Adapted Transformer Neural Network and FFT-Based Features Extraction, *Sensors*, Vol. 25, No. 3, 1–19. doi:10.3390/s25030652.
24. A, S., Christo, M. S., and Elizabeth, J. V. (2025). A Hybrid Approach to Time Series Forecasting: Integrating ARIMA and Prophet for Improved Accuracy, *Results in Engineering*, Vol. 27, No. 2, 105–121. doi:10.1016/j.rineng.2025.105703.
25. Navodya Gimhani Ranasinghe, A., Saeed, N., and Sadeghian, P. (2026). Comparative Analysis of LSTM and SARIMA for Global Temperature Forecasting: Impact of Regional Trends and Emissions, *Climate*, Vol. 14, No. 3, 1–22. doi:10.3390/cli14030072.
26. Natisharevi, R. J., Rizal, J., Firdaus, F., Novianti, P., and Lestari, W. A. (2025). Comparative Analysis of SARIMA, FFNN, and Hybrid Models for Sea Surface Temperature Prediction at Enggano Island (2018–2024), *JURNAL GEOCELEBES*, Vol. 9, No. 2, 189–212. doi:10.70561/geocelebes.v9i2.46445.
27. NASA. (2024). NASA POWER | Prediction Of Worldwide Energy Resources.
28. Tokan, L. F., and Hermawan, A. (2023). Implementasi Model SARIMA Untuk Memprediksi Produksi Minyak Kelapa Sawit, *Jurnal Fasilkom*, Vol. 13, No. 3, 456–463. doi:10.37859/jf.v13i3.6033.
29. Christie, G., Hatidja, D., and Tumilaar, R. (2022). Penerapan Metode SARIMA Dalam Model Intervensi Fungsi Step Untuk Memprediksi Jumlah Pegunjung Objek Wisata Londa, *Jurnal Ilmiah Sains*, Vol. 22, No. 2, 96–103. doi:10.35799/jis.v22i2.40961.
30. Anbiya, W., and Garini, F. C. (2022). Application of GARCH Forecasting Method in Predicting The Number of Rail Passengers (Thousands of People) in Jabodetabek Region, *Jurnal Matematika, Statistika & Komputasi*, Vol. 18, No. 2, 198–223. doi:10.20956/j.v18i2.18382.
31. Atkinson, A. C., Riani, M., and Corbellini, A. (2021). The Box–Cox Transformation: Review and Extensions, *Statistical Science*, Vol. 36, No. 2, 1–14. doi:10.1214/20-STS778.
32. Wanjuki, T. M., Wagala, A., and Muriithi, D. K. (2021). Forecasting Commodity Price Index of Food and Beverages in Kenya Using Seasonal Autoregressive Integrated Moving Average (SARIMA) Models, *European Journal of Mathematics and Statistics*, Vol. 2, No. 6, 50–63. doi:10.24018/ejmath.2021.2.6.80.
33. Punyapornwithaya, V., Mishra, P., Sansamur, C., Pfeiffer, D., Arjkumpa, O., Prakotcheo, R., Damrongwatanapokin, T., and Jampachaisri, K. (2022). Time-Series Analysis for the Number of Foot and Mouth Disease Outbreak Episodes in Cattle Farms in

Thailand Using Data from 2010–2020, *Viruses*, Vol. 14, No. 7, 1–14. doi:10.3390/v14071367.

34. Spiliotis, E., and Petropoulos, F. (2023). On the Disagreement of Forecasting Model Selection Criteria, *MDPI*, Vol. 5, No. 2, 487–498.

35. St-aubin, P., and Agard, B. (2022). Precision and Reliability of Forecasts Performance Metrics, *MDPI*, Vol. 4, No. 4, 882–903.

36. Agiakloglou, C., and Tsimpanos, A. (2023). *Evaluating the Performance of AIC and BIC for Selecting Spatial Econometric Models*, *Journal of Spatial Econometrics* (Vol. 4), Springer International Publishing. doi:10.1007/s43071-022-00030-x.

37. de Myttenaere, A., Golden, B., Le Grand, B., and Rossi, F. (2016). Mean Absolute Percentage Error for Regression Models, *Neurocomputing*, Vol. 192, No. 1, 38–48. doi:10.1016/j.neucom.2015.12.114.

38. Hewamalage, H., Ackermann, K., and Bergmeir, C. (2023). Forecast Evaluation for Data Scientists: Common Pitfalls and Best Practices, *Data Mining and Knowledge Discovery*, Vol. 37, No. 2, 788–832. doi:10.1007/s10618-022-00894-5.

39. As-syakur, A. R., Osawa, T., Miura, F., Nuarsa, I., Ekayanti, N. W., Bagus, I., Dharma, S., Adnyana, I. S., Arthana, I., and Tanaka, T. (2016). Maritime Continent Rainfall Variability during the TRMM Era: The Role of Monsoon, Topography and El Niño Modoki, *Dynamics of Atmospheres and Oceans*, Vol. 75, No. 1, 58–77. doi:10.1016/j.dynatmoce.2016.05.004.

40. Navodya, A., Ranasinghe, G., and Saeed, N. (2026). Comparative Analysis of LSTM and SARIMA for Global Temperature Forecasting : Impact of Regional Trends and Emissions, *MDPI*, Vol. 14, No. 72, 1–22.

41. Alekseev, G., Soldatenko, S., Glok, N., Kharlanenkova, N., Angudovich, Y., and Smirnov, M. (2025). Tropical Sea Surface Temperature and Sea Level as Candidate Predictors for Long-Range Weather and Climate Forecasting in Mid-to-High Latitudes, *MDPI*, Vol. 13, No. 84, 1–11.